AIAA-98-4803

HSCT CONFIGURATION DESIGN SPACE EXPLORATION USING AERODYNAMIC RESPONSE SURFACE APPROXIMATIONS

Chuck A. Baker*, Bernard Grossmanå, Raphael T. Haftkaç, William H. Mason§, and Layne T. Watson¶

Multidisciplinary Analysis and Design (MAD) Center for Advanced Vehicles
Virginia Polytechnic Institute and State University
Blacksburg, Virginia 24061-0203

Abstract

A method has been developed to generate and use polynomial approximations to the range and cruise drag components in a highly constrained, multidisciplinary design optimization of a High Speed Civil Transport configuration. The method improves optimization performance by eliminating the numerical noise present in the analyses through the use of response surface methodology. In our implementation, we fit quadratic polynomials within variable bounds to data gathered from a series of numerical analyses of different aircraft designs. Because the HSCT optimization process contains noise and suffers from a nonconvex design space even when noise is filtered out, multiple optimization runs are performed from different starting points with and without the response surface models in order to evaluate their effectiveness. It is shown that response surface methodology facilitates design space exploration, allowing improvements in terms of both convergence performance and computational effort when multiple starting points are required.

1. Introduction

Numerical noise is a critical issue in the field of multidisciplinary design optimization (MDO). Numerical noise occurs as a result of the incomplete convergence of iterative processes, round-off errors, and the discrete representation of continuous physical objects [1, 2]. Such numerical noise is typically manifested as a low amplitude, high frequency variation in the results obtained from computer analyses as the design parameters vary. When gradient based numerical optimization is attempted, this oscillatory behavior creates numerous, artificial local optima and causes slow convergence or even convergence failures [1, 3].

In the MDO of a high speed civil transport (HSCT), numerical noise is present in the analyses of various disciplines, with the majority of the noise originating from aerodynamic computations. In our studies numerical noise was most evident in the calculation of drag coefficients which subsequently lead to noise in the calculation of range.

Previous work using a variable complexity modeling (VCM) approach [3, 4, 5, 6] encountered the noise problem, and was unsuccessful in solving it. This approach used computationally cheap low fidelity models and computationally expensive high fidelity models in a method that reduced the computational effort to an acceptable level. The low fidelity models were also much smoother. At each optimization cycle the low fidelity predictions were corrected using a scaling factor obtained from the expensive methods. The VCM approach was successful in reducing CPU time and jumping over some of the artificial local minima due to noise, but occasionally failed because erratic calculations of scaling factors at the peaks and troughs of the noise lead to convergence problems. VCM was also problematic in that the low fidelity models are based on several geometric assumptions that restrict the optimizer from venturing into otherwise available regions of the design space.

A somewhat different approach to numerical noise is Kelly's implicit filtering [7], which has been very successful for low dimensional problems here the noise can be characterized with constant parameters. Its application to MDO problems where the noise characteristics vary across the constraints and across the design space is not so clear, but its performance on low dimensional HSCT MDO problems is comparable to that of response surfaces [8].

More recent work to eliminate the noise employs response surface methodologies (RSM). RSM [9, 10, 11] uses simple mathematical models, typically low-order polynomials, to approximate the response and

---

* Graduate Research Assistant, Dept. of Aerospace and Ocean Engineering.
å Professor and Dept. Head of Aerospace and Ocean Engineering, Associate Fellow AIAA.
ç Professor of Aerospace Engineering, Mechanics and Engineering Science, University of Florida, Gainesville, FL, Fellow AIAA.
§ Professor of Aerospace and Ocean Engineering, Associate Fellow AIAA.
¶ Professor of Computer Science and Mathematics.

smooth out numerical noise present in the analyses. Such RS models are created using a limited number of analyses at a set of statistically selected points in the design space. The time consumed by running these initial analyses is considered an investment in the future use of the RS models, with the understanding that the optimization performance will be increased sufficiently enough for the RS models to be beneficial if a certain number of optimizations are executed.

HSCT optimizations have been conducted using aerodynamic RS models for smaller regions of the design space with success [12]. The purpose of this work is to construct RS models that cover a larger volume of the design space and evaluate the effectiveness of these models as a design space exploration tool by running optimizations from a wide variety of starting points.

2. The HSCT Design Problem

The design problem considered is the optimization of a HSCT configuration [13, 14] to minimize takeoff gross weight (TOGW) for a range of 5500 nautical miles and a cruise Mach number of 2.4, while carrying 251 passengers. The choice of gross weight as the objective function directly incorporates both aerodynamic and structural considerations, in that the structural design directly affects aircraft empty weight and drag, while aerodynamic performance dictates drag and thus the required fuel weight.

To successfully perform aircraft configuration optimization, it is very important to have a simple, but meaningful, mathematical characterization of the geometry of the aircraft. This paper uses a model that defines the HSCT design problem using the twenty-eight design variables listed in Table 1. Twenty-four of the design variables describe the geometry of the aircraft and can be divided into six categories: wing planform, airfoil shape, tail areas, nacelle placement, and fuselage shape. In addition to the geometric parameters, four variables define the idealized cruise mission: mission fuel, engine thrust, initial cruise altitude, and constant climb rate used in the range calculation.

Sixty-eight geometry, performance, and aerodynamic constraints, listed in Table 2, are included in the optimization. Aerodynamic and performance constraints can only be assessed after a complete analysis of the HSCT design; however, the geometric constraints can be evaluated using algebraic relations based on the 28 design variables. In the evaluation of the range constraint is where the numerical noise from the aerodynamic analyses is evident.

Table 1. HSCT configuration design variables.

D.V.	Decription
1	wing root chord (ft)
2	LE break, x (ft)
3	LE break, y (ft)
4	TE break, x (ft)
5	LE wing tip, x (ft)
6	wing tip chord (ft)
7	wing semispan (ft)
8	location airfoil max. thickness
9	LE radius parameter
10	t/c at wing root
11	t/c at LE break,
12	t/c at wing tip
13	fuselage axial restraint #1 (ft)
14	fuselage radius at axial restraint #1 (ft)
15	fuselage axial restraint #2 (ft)
16	fuselage radius at axial restraint #2 (ft)
17	fuselage axial restraint #3 (ft)
18	fuselage radius at axial restraint #3 (ft)
19	fuselage axial restraint #4 (ft)
20	fuselage radius at axial restraint #4 (ft)
21	location of inboard nacelle (ft)
22	location of outboard nacelle (ft)
23	mission fuel weight (lbs)
24	starting cruise altitude (ft)
25	cruise climb rate (ft/min)
26	vertical tail area (ft²)
27	horizontal tail area (ft²)
28	thrust per engine (lbs)

Table 2. HSCT optimization constraints.

#	Description
1	Range ≥ 5,500 n.mi.
2	Required C_L at landing speed ≤ 1
2-30	Section C_l ≤ 2
21	Landing angle of attack ≤ 12°
22	Fuel volume ≤ half of wing volume
23	Spike prevention
24-41	Wing chord ≥ 7.0 ft.
42-43	No engine scrape at landing angle-of-attack
44-45	No engine scrape at landing angle-of-attack, with ° roll
46	No wing tip scrape at landing
47	Rudder deflection for crosswind landing ≤ 22.5°
48	Bank angle for crosswind landing ≤ 5°
49	Takeoff rotation to occur ≤ 5 sec
50	Tail deflection for approach trim ≤ 22.5°
51	Wing root T.E. ≤ horiz. tail L.E.
52	Balanced field length ≤ 11,000 ft
53	T.E. break scrape at landing with ° roll
54	L.E. break ≤ semispan
55	T.E. break ≤ semispan
56-58	Root, break, tip t/c ≥ 1.5%
59	Fuselage: $x_{rest1} \geq 5$ft
60	Fuselage: $x_{rest1} + 10\text{ft} \leq x_{rest2}$
61	Fuselage: $x_{rest2} + 10\text{ft} \leq x_{rest3}$
62	Fuselage: $x_{rest3} + 10\text{ft} \leq x_{rest4}$
63	Fuselage: $x_{rest4} + 10\text{ft} \leq 300\text{ft}$
64	Nacelle 1, y ≥ side-of-body
65	Nacelle 1, y ≤ nacelle 2, y
66	Engine-out limit with vertical tail design; otherwise 50%
67-68	Maximum thrust required ≤ available thrust

The analysis methods used to calculate the three drag components (C_{Dwave}, $C_{L\alpha}$, and C_T/C_L^2) used in the drag calculation and their corresponding ranges are described in References 5, 15, 16. The aerodynamics calculations are based on the Mach box method [17, 18], and the Harris wave drag code [19]. A simple strip boundary layer friction estimate is implemented as in [5]. A vortex lattice method with vortex lift and ground effects included [20] is used to calculate landing angle of attack.

All optimizations were performed on a SGI Power Challenge using the modified method of feasible directions algorithm in the optimization software package DOT [21]. If the RS model optimum design violates the range constraint calculated by exact analyses by a small amount, it is sometimes possible to add fuel to the aircraft to increase the range without violating any other constraints. When this is done, the aircraft TOGW used for comparison is replaced by the corrected take-off gross weight (CTOGW) that includes the added fuel weight.

3. Construction of RS Models

The RSM process begins with the selection of a central (or baseline) design. The central design becomes the centroid of a box over which the RS model is created. The central design for this work was chosen to be an optimum design that was achieved using variable complexity modeling (VCM). The initial (starting pt. A) and optimal performance data for this optimization are listed in Table 3 and the corresponding planform shapes are shown in Figure 1.

Table 3. Performance data for VCM optimization run (starting pt. A).

	Initial	VCM Optimum
Range, RS (n. mi.)	---	---
Range, Exact (n. mi.)	5,607	5,500
TOGW (lbs)	805,955	750,350
CTOGW (lbs)	---	750,350
CPU Time (min.)	---	184
Active Side Constraints	---	---

The next step in the RSM process involves the definition of variable bounds. Ideally the bounds would be selected to give the greatest volume to allow a wide variation in the design parameters. However, as the design *box* becomes large, the maximum error in the quadratic RS model also grows. The goal here is to have a design *box* that provides a significant amount of variation in designs while keeping errors acceptable. For this study, the variable bounds were set at ±15% of the baseline values of each design variable.

With the design *box* defined, a design sample set is generated. Initially, two different methods were used in the construction of the data set. One of the data sets is an orthogonal array created using a method by Bose [22] consisting of 47 levels for a total of 2209 points. The other data set is a small composite design (SCD) [11] consisting of 2105 points (a 2048 SCD plus face points and the central design). The number of points in each design set is then slightly decreased by the removal of geometrically impossible designs. The impossible designs include configurations with negative chords that arise from a combination of extreme design variable values that occurs at certain vertices of the design *box*. Only 3 designs were removed from the 2209 point orthogonal array, while 512 were eliminated from the 2105 point SCD-based data set. Since such a large number of points were removed from the SCD, an additional SCD was created for a box with ±7.5% variable bounds, providing a second level of points. The total number of points remaining was 2206 for the orthogonal array and 2617 for the SCD-based set after pruning.

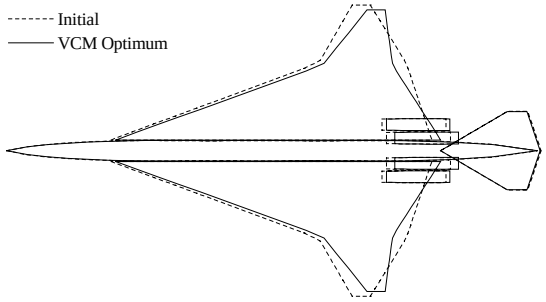

Figure 1. Planform shapes for VCM optimization run (starting pt. A).

Once the design set has been pruned, the analyses are run for each point and the RS models can be generated. A total of four RS models are generated for the aerodynamics. Since the noise is seen primarily in the range constraint, it was decided to approach this problem from two directions: to model the range itself as a function of the 28 design variables and to model the individual drag components used to calculate the range as a function of the 28 design variables. The aerodynamic calculations took 597 CPU minutes to analyze the 2206 point set and 685 CPU minutes for the 2617 point set on the Power Challenge.

The statistical software SAS [23] is used to create all of the RS models, which are quadratic least square fits of the sample design set data. The error of each RS model's range calculated at the design points is listed in Table 4. As can be seen from the Table, the orthogonal

array RS models have smaller errors compared to those of the SCD set. For this reason, the orthogonal array RS models were selected for use in this optimization study. The space filling ability of orthogonal arrays also makes more physical sense than the SCD that is composed of design *box* vertices, since most of the feasible design space exists near the center of the *box* and not around the edges.

Table 4. Errors of RS models.

Error (n. mi.)	Orthogonal Array		SCD-based Data Set	
	Range RS	Drag RS Range	Range RS	Drag RS Range
median	24	17	39	21
rms	46	31	63	36

Table 5. Performance data for VCM and RS model optimization runs (starting pt. A).

	Initial	VCM Optimum	Range RS Optimum	Drag RS Optimum
Range, RS (n. mi.)	---	---	5,500	5,500
Range, Exact (n. mi.)	5,607	5,500	5,522	5,481
TOGW (lbs)	805,955	750,350	768,859	761,836
CTOGW (lbs)	---	750,350	766,879	763,546
CPU Time (min.)	---	184	45	30
Active Side Constraints	---	none	none	none

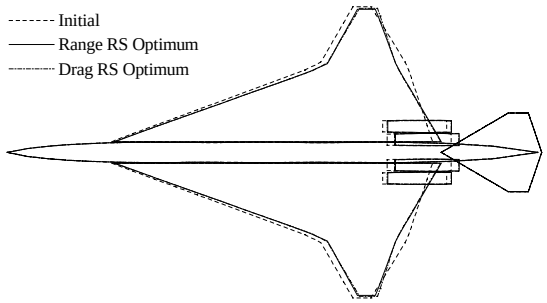

Figure 2. Planform shapes for RS model optimization runs (starting pt. A).

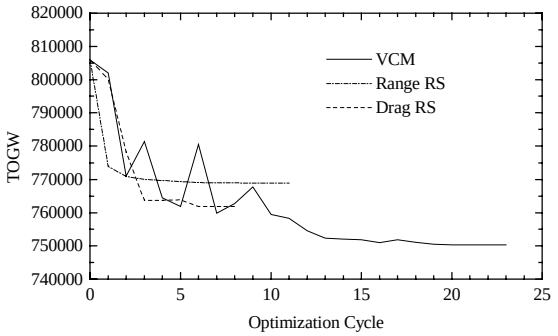

Figure 3. Convergence histories for optimization runs (starting pt. A).

4. Optimization from Multiple Starting Points

The first RS model optimization run was conducted from starting point A, the same starting point as the VCM optimization that produced the central design. The performance data for these optimizations are listed in Table 5. The resulting planform shapes and convergence histories are shown in Figures 2 and 3, respectively.

Table 6. Performance data for VCM and RS model optimization runs (starting pt. B).

	Initial	VCM Optimum	Drag RS Optimum
Range, RS (n. mi.)	---	---	5,500
Range, Exact (n. mi.)	4,946	5,500	5,463
TOGW (lbs)	823,331	791,066	789,386
CTOGW (lbs)	---	791,066	792,716
CPU Time (min.)	---	326	56
Active Side Constraints	---	none	none

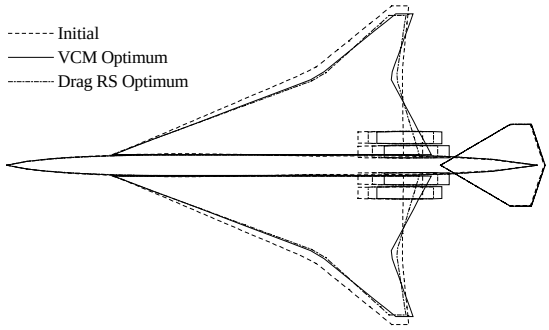

Figure 4. Planform shapes for VCM and RS model optimization runs (starting pt. B).

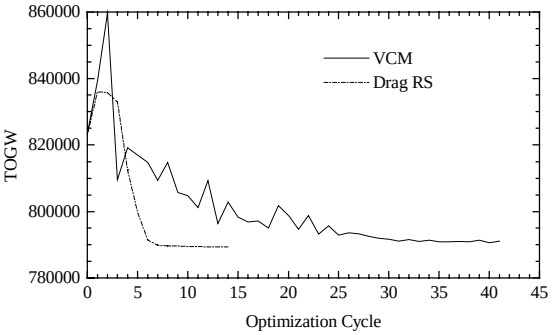

Figure 5. Convergence histories for optimization runs (starting pt. B).

For the optimum designs, the range RS model under-predicted the exact range by 22 nautical miles and the range calculated using drag RS models was 19 miles short of the exact range. The sets of models yielded a similar optimum, while using only 25% of the time needed for the VCM optimization. The

convergence history of the VCM also shows a slow, noisy convergence when compared to those of the RS models. The VCM optimization not only takes twice as many cycles to converge, the cycles are twice as long due to the multifidelity calculations.

Table 7. Performance data for VCM and RS model optimization runs (starting pt. C).

	Initial	VCM Optimum	Drag RS Optimum
Range, RS (n. mi.)	---	---	5,500
Range, Exact (n. mi.)	4,621	5,500	5,478
TOGW (lbs)	795,161	765,751	756,515
CTOGW (lbs)	---	765,751	758,495
CPU Time (min.)	---	293	98
Active Side Constraints	---	max. vert. tail area	max. vert. tail area

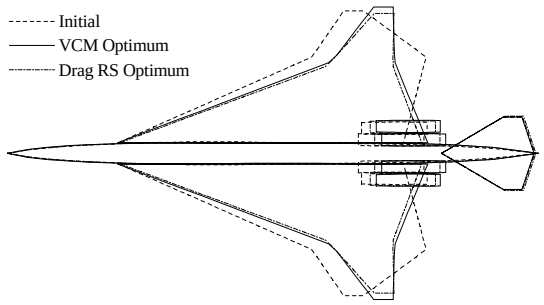

Figure 6. Planform shapes for VCM and RS model optimization runs (starting pt. C).

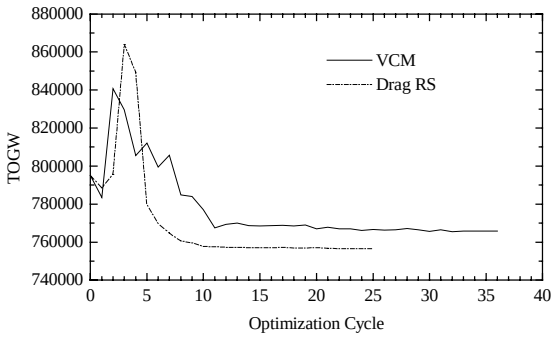

Figure 7. Convergence histories for optimization runs (starting pt. C).

For the remainder of the optimization runs, the single range RS model was abandoned in favor of the drag RS models. This was done to simplify comparison of the results, providing a single RS optimum for every VCM optimum. The drag RS models were chosen because they had slightly smaller errors (Table 4) and because it was felt that the individual drag components, being at a more fundamental level, are better modeled by a quadratic function of the 28 design variables than their resulting range.

A total of four more starting points were used to explore the design space. The starting points were selected primarily for their variety, with starting point B representing a conventional HSCT design and the other points being considerably more unorthodox. Details of optimizations from starting points B, C, D, and E are shown in Figures 4 to 11 and Tables 6 to 9.

Table 8. Performance data for VCM and RS model optimization runs (starting pt. D).

	Initial	VCM Optimum	Drag RS Optimum
Range, RS (n. mi.)	---	---	5,500
Range, Exact (n. mi.)	5,295	5,500	5,472
TOGW (lbs)	872,763	733,785	743,431
CTOGW (lbs)	---	733,785	745,951
CPU Time (min.)	---	218	51
Active Side Constraints	---	none	none

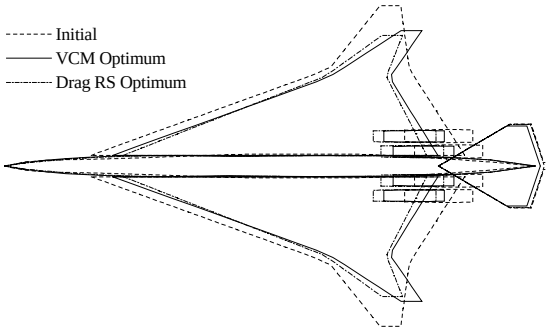

Figure 8. Planform shapes for VCM and RS model optimization runs (starting pt. D).

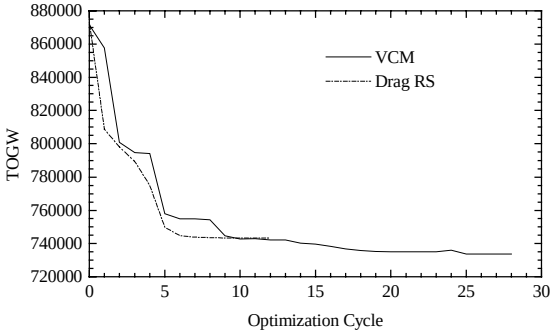

Figure 9. Convergence histories for optimization runs (starting pt. D).

Starting points B and C resulted in essentially the same optimum design independently of the method used. The discrepancies in the optimum weights can be attributed to small differences in the optimal airfoil design variables.

The optimum designs obtained from starting point D show a little more diversity between them and are by far the lightest designs achieved. The biggest difference in these two designs is the size of the horizontal tail. The

RS model optimum has a much larger horizontal tail and is consequentially much heavier. Other notable differences between these two designs are the length of the root chord and the sweep of the outboard section of the wing.

Table 9. Performance data for VCM and RS model optimization runs (starting pt. E).

	Initial	VCM Optimum	Drag RS Optimum
Range, RS (n. mi.)	---	---	5,500
Range, Exact (n. mi.)	4,316	5,500	5,464
TOGW (lbs)	769,080	766,249	770,256
CTOGW (lbs)	---	766,249	773,496
CPU Time (min.)	---	146	44
Active Side Constraints	---	none	none

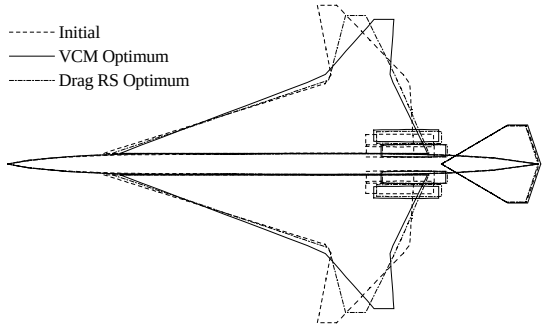

Figure 10. Planform shapes for VCM and RS model optimization runs (starting pt. E).

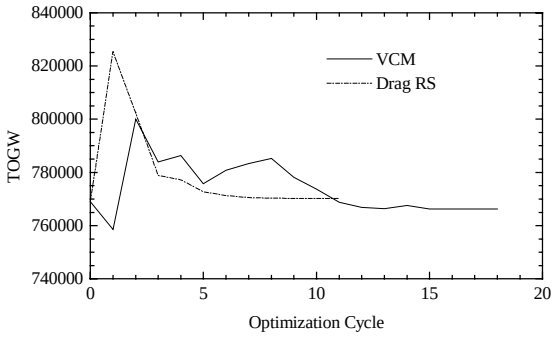

Figure 11. Convergence histories for optimization runs (starting pt. E).

For starting points A and E, the VCM and RS model optimum designs have very different weights. The only major difference seen in designs is the sweep of the outboard section of the wing. In both cases the RS model converges at a design that has an outboard sweep angle roughly halfway between that of the initial and optimal VCM design. This difference leads to the RS model designs being more than 10,000 lbs heavier than the VCM optimum.

Again, a distinct difference between the two methods can be seen in the convergence history and CPU time used for each optimization. In all cases the optimization using RS models moved swiftly and smoothly to their optimum while the VCM approach's convergence is visibly hindered by the presence of noise. Because of the smooth convergence and short function evaluation time, the RS model optimizations converged 76% faster on average, in terms of CPU time, than the VCM optimizations.

The drag RS models also proved to be highly accurate in all of the optimizations. The maximum error seen in the range calculated using the drag RS models at any of the optima was only 37 nautical miles.

From all of the starting points, the optimizer was successful in overcoming a large initial range deficit to produce a lighter, feasible design whether using the VCM approach or RS models. The best optimum design for each method came from starting point D, where the VCM approach produced a design with a TOGW of 733,785 lbs and the RS models produced a design with a TOGW of 745,951 lbs. A compilation of optimum design variables and performance data for all of the optimization runs is given in Table 10.

5. Discussion

In the five HSCT configuration optimizations that were performed, we were able to see the advantages and disadvantages of quadratic RS models. In our implementation, RSM has the advantage of accurate noise filtering and computational efficiency over the VCM approach when using a sufficient number starting points. However, the VCM approach has the advantage of not being confined to a design *box* as well as the ability to jump through the design space toward promising regions.

The values of range predicted by the drag RS models were exceptionally accurate over the entire design *box*. The RS models were also able to capture the governing trends of the exact values of range (excluding the noise) since most of the optimizations started from the same initial design were able to find very similar optimum designs whether the VCM approach or RS models were used.

The biggest gain in using the RS models for design space exploration is not necessarily in the optimum that is found, but in how efficiently this optimum is found. Even though there is an initial investment of almost 600 CPU minutes put into the construction of the RS models, the increase in optimization performance using the RS models over the five optimization runs from different starting conditions can be seen in Figure 12. In this case, after three optimizations were performed the total CPU time used by RS model optimizations was

Table 10. Optimum design variables and performance data from all optimization starting points.

Parameter	VCM Optima					Drag RS Model Optima				
	A	B	C	D	E	A	B	C	D	E
wing root chord (ft)	183.6	179.6	175.1	183.7	173.7	184.6	173.5	170.1	171.4	178.9
LE break, x (ft)	116.9	114.8	120.7	121.9	115.1	119.6	117.9	116.5	114.0	122.4
LE break, y (ft)	41.6	42.7	44.9	43.2	42.9	42.1	42.7	42.5	43.9	40.7
TE break, x (ft)	156.5	156.4	156.4	156.5	152.3	159.3	160.7	153.9	148.6	161.1
LE wing tip, x (ft)	141.9	159.5	144.6	163.0	143.4	137.2	156.7	143.4	146.2	131.8
wing tip chord (ft)	10.3	9.8	11.0	11.8	11.2	10.2	9.4	11.1	11.6	11.3
wing semispan (ft)	72.3	78.2	75.3	69.3	74.4	73.5	77.4	71.7	66.7	76.6
location airfoil max. thickness	0.491	0.491	0.494	0.500	0.492	0.495	0.524	0.498	0.561	0.487
LE radius parameter	2.95	2.82	2.52	3.34	3.00	2.96	2.81	2.60	3.33	3.00
t/c at wing root	0.0232	0.0247	0.0259	0.0236	0.0249	0.0237	0.0255	0.0262	0.0242	0.0259
t/c at LE break,	0.0173	0.0181	0.0160	0.0191	0.0180	0.0175	0.0187	0.0159	0.0196	0.0180
t/c at wing tip	0.0150	0.0154	0.0161	0.0169	0.0159	0.0158	0.0150	0.0172	0.0172	0.0162
fuselage axial restraint #1 (ft)	2.8	3.1	2.7	2.5	2.8	3.2	2.3	3.2	2.3	2.9
fuselage radius at restraint #1 (ft)	0.63	0.64	0.54	0.56	0.67	0.66	0.72	0.53	0.70	0.58
fuselage axial restraint #2 (ft)	14.1	16.0	14.0	15.5	15.5	14.4	16.3	13.2	16.3	13.7
fuselage radius at restraint #2 (ft)	2.48	2.75	2.54	2.47	2.50	2.61	2.63	2.25	2.11	2.12
fuselage axial restraint #3 (ft)	114.5	111.1	120.0	128.2	122.3	111.7	109.0	116.2	131.6	126.3
fuselage radius at restraint #3 (ft)	5.60	5.69	5.61	5.32	5.45	5.50	5.77	5.71	5.60	5.37
fuselage axial restraint #4 (ft)	178.8	171.0	165.3	195.6	190.2	181.4	167.8	171.6	193.8	193.1
fuselage radius at restraint #4 (ft)	5.53	5.53	5.45	5.71	5.64	5.42	5.47	5.58	5.76	5.69
location of inboard nacelle (ft)	7.00	7.50	7.46	7.89	7.41	7.08	7.54	7.56	8.06	7.33
location of outboard nacelle (ft)	14.45	15.25	14.94	16.47	15.71	14.42	15.34	14.56	16.47	14.71
mission fuel weight (lbs)	386,666	408,497	396,397	380,357	397,152	394,834	406,911	390,581	388,345	396,675
starting cruise altitude (ft)	58,949	58,845	58,830	57,640	59,111	58,680	58,994	59,624	58,395	59,212
climb rate (ft/min)	37.5	37.1	37.3	36.1	38.1	37.4	37.2	37.9	37.7	37.5
vertical tail area (ft^2)	443.8	465.3	509.9	486.9	452.3	454.9	460.9	510.0	496.5	446.3
horizontal tail area (ft^2)	729.9	809.3	632.4	767.6	728.1	744.5	805.1	657.1	828.6	691.7
thrust per engine (lbs)	4,866	5,086	4,941	4,405	5,062	4,883	5,114	5,121	4,728	5,061
Range, RS (n.mi.)	---	---	---	---	---	5,500	5,500	5,500	5,500	5,500
Range, Exact (n. mi.)	5,500	5,500	5,500	5,500	5,500	5,481	5,463	5,478	5,472	5,464
TOGW (lbs)	750,350	791,066	765,751	733,785	766,249	761,836	789,386	756,515	743,431	770,256
CTOGW (lbs)	750,350	791,066	765,751	733,785	766,249	763,546	792,716	758,495	745,951	773,496
Cycles	23	41	36	28	18	8	14	23	12	11
CPU Time (min.)	184	326	293	218	146	30	56	98	51	44
Active Side Constraints	none	none	max. vert. tail area	none	none	none	none	max. vert. tail area	none	none

surpassed by that of conventional optimizations using VCM.

While the results obtained for starting points B and C were virtually identical, the VCM optimization is able to make substantial improvements over the RS models for the other three starting points. These improvements are most likely due to the behavior of the VCM approach during an individual optimization cycle. Since VCM uses low fidelity analyses with some initially calculated correction factor, it is possible, as each optimization cycle progresses, for it to jump through constraints that exist in the high fidelity analyses and RS models. For example, the RS model optimization from starting point A begins by following the path of the VCM optimization until the RS models encounter a local minimum due to the range constraint. The VCM optimization continues on to reduce the weight by an additional 13,000 lbs to converge at an optimal weight of 750,350 lbs. If a RS model optimization is then transplanted into this better region of the design space and started from the VCM optimum, it is able to converge at a feasible design similar to the VCM optimization, weighing 752,810 lbs. In this case, the VCM approach was able to move to a region of the design space that is better than what it started in.

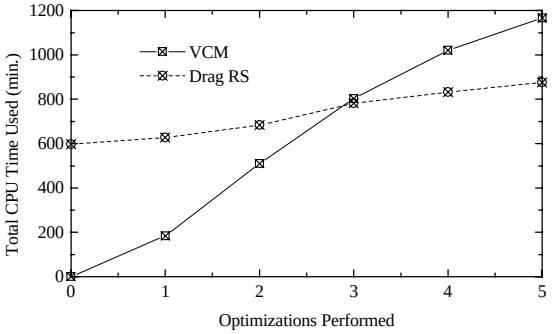

Figure 12. Comparison of total CPU time used for VCM and RS model optimizations.

6. Concluding Remarks

The use of RS models in this study was valuable in providing a relatively quick and accurate means of

exploring the design space. The large size of the design *box* that was used is evident in the variety of initial designs that were available for optimization. The spaciousness of the design *box* can also be seen in the fact that the side constraints did not play an important role in the optimization process.

When performing design space exploration in a nonconvex space without the aid of a global optimizer, multiple starting points are required with or without RS models. In this case, the RSM used was successful in filtering out the effects of noise while providing savings of almost 5 hours of CPU time when compared to the VCM approach. Alternatively, the VCM approach was successful in navigating to better regions of the design space.

In addition to other research conducted with higher fidelity aerodynamic RS models [24], work has been done on structural RS models for a HSCT configuration optimization over a small design *box* [25]. Work is currently in progress to use the RSM presented to construct structural RS models for the large design *box* used in this study. The ultimate goal here is to use both the aerodynamic and the structural RS models together in a HSCT configuration optimization.

Acknowledgements

Support for this research effort was provided through the NASA Langley Research Center grants NAG1-1160 and NAG1-1562.

References

[1] Giunta, A. A., Dudley, J. M., Grossman, B., Haftka, R. T., Mason, W. H., and Watson, L. T. ôNoisy Aerodynamic Response and Smooth Approximations in HSCT Design," AIAA Paper 94-4376, Sept. 1994.

[2] Venter, G., Haftka, R. T., and Starnes, J. H. "Construction of Response Surfaces for Design Optimization Applications," in *Proceedings of the 6th AIAA/NASA/ISSMO Symposium on Multidisciplinary Analysis and Optimization*, pp. 548-564, Bellevue, WA, AIAA Paper 96-4040 (Sept. 1996).

[3] Dudley, J., Huang, X., MacMillin, P. E., Grossman, B., Haftka, R. T., and Mason, W. H. "Multidisciplinary Optimization of the High-Speed Civil Transport," AIAA Paper 95-0124 (1995).

[4] Hutchison, M. G., Unger, E. R., Mason, W. H., Grossman, B.,and Haftka, R. T. "Aerodynamic Optimization of an HSCT Configuration Using Variable-Complexity Modeling," AIAA Paper No. 93-0101, January 1993.

[5] Hutchison, M. G., Unger, E. R., Mason, W. H., Grossman, B.,and Haftka, R. T. ôVariable-Complexity Aerodynamic Optimization of a High-Speed Civil Transport Wing,ö *Journal of Aircraft*, 31, No. 1: 110-116, 1994.

[6] Dudley, J., Huang, X., Haftka, R. T., Grossman, B., and Mason, W. H. ôVariable-Complexity Interlacing of Weight Equation and Structural Optimization of the High-Speed Civil Transport,ö AIAA Paper No.94-4377, September 1994.

[7] Gilmore, P. and Kelley, C. T. ôAn Implicit Filtering Algorithm for Optimization of Functions with Many Local Minima," SIAM J. Opt., 5(2), 269-285 (1995).

[8] Giunta, A. A. Aircraft Multidisciplinary Design Optimization Using Design of Experiments Theory and Response Surface Modeling Methods, Ph.D. thesis, Virginia Polytechnic Institute and State University, 1997.

[9] Box, G. E. P. and Wilson, K. B. ôOn the Experimental Attainment of Optimum Conditions," *Journal of Royal Statistical Society*, vol. B13, pp. 38-45, 1951.

[10] Box, G. E. P., Hunter, W. G., and S., H. J. *Statistics for Experiments: An Introduction to Design, Data Analysis, and Model Building*, pp. 78-83. New York, N. Y.: John Wiley & Sons, 1978.

[11] Myers, R.H. and Montgomery, D. C. *Response Surface Methodology: Process and Product Optimization Using Designed Experiments*, pp. 650-651. New York, N. Y.: John Wiley & Sons, 1995.

[12] Golovidov, O. ôVariable-Complexity Response Surface Approximations for Aerodynamic Parameters in HSCT Optimization," Tech. Rep. MAD 97-06-01, VPI&SU, Blacksburg, VA, June 1997.

[13] MacMillin, P., Golovidov, O., Mason, W., Grossman, B., and Haftka, R. ôTrim, Control and Performance Effects in Variable-Complexity High-Speed Civil Transport Design," Tech. Rep. MAD 96-07-01, VPI&SU, Blacksburg, VA, July 1996.

[14] MacMillin, P. E., Golovidov, O. B., Mason, W. H., Grossman, B., and Haftka, R. T. ôAn MDO Investigation of the Impact of Practical Constraints on an HSCT Optimization," AIAA Paper 97-0098, Jan. 1997.
[15] Hutchison, M. G., Huang, X., Mason, W. H., Haftka, R. T., and Grossman, B. ôVariable-Complexity Aerodynamic-Structural Design of a High-Speed Civil Transport Wing," AIAA Paper 92-4695, Sept. 1992.
[16] Hutchison, M. G., Mason, W. H., Grossman, B., and Haftka, R. T. ôAerodynamic Optimization of an HSCT Configuration Using Variable-Complexity Modeling," AIAA Paper 93-0101, Jan. 1993.
[17] Carlson, H., Mack, R., and Barger, R. ôEstimation of Attainable Leading Edge Thrust for Wings at Subsonic and Supersonic Speeds," NASA TP-1500, 1979.
[18] Carlson, H. and Miller, D. ôNumerical Methods for the Design and Analysis of Wings at Supersonic Speeds," NASA TN D-7713, 1974.
[19] Harris, Jr., R. V. ôAn Analysis and Correlation of Aircraft Wave Drag," NASA TM X-947, 1964.
[20] Bertin, J. and Smith, M. *Aerodynamics for Engineers*, pp. 261-282. Prentice Hall, 2nd ed., 1989.
[21] Vanderplaats Research & Development, Inc. *DOT Users Manual, Version 4.20*, Colorado Springs, CO, 1995.
[22] Bose, R.C. *Sankhya, Volume 3*, pp. 323-338. 1938
[23] SAS Institute, Inc. *SAS/STAT UserÆs Guide, Version 6*, Cary, NC, 1995.
[24] Knill, D. L., Giunta, A. A., Baker, C. A., Grossman, B., Mason, W. H., Haftka, R. T. and Watson, L. T. ôHSCT Configuration Design Using Response Surface Approximations of Supersonic Euler Aerodynamics,ö AIAA Paper No. 98-0905, *Presented at the Thirty-sixth Aerospace Sciences Meeting & Exhibi* , Reno, NV, January 1998.
[25] Balabanov, V. O. *Development of Approximations for HSCT Wing Bending Material Weight Using Response Surface Methodology*, Ph.D. thesis, Department of Aerospace and Ocean Engineering, Virginia Polytechnic Institute and State University, 1997.